nature medicine

The long noncoding RNA *Chaer* defines an epigenetic checkpoint in cardiac hypertrophy

Zhihua Wang[1–4], Xiao-Jing Zhang[1–3], Yan-Xiao Ji[1–3], Peng Zhang[1–3], Ke-Qiong Deng[1–3], Jun Gong[1–3], Shuxun Ren[4], Xinghua Wang[5], Iris Chen[4], He Wang[4], Chen Gao[4], Tomohiro Yokota[4], Yen Sin Ang[6,7], Shen Li[8,9], Ashley Cass[10,11], Thomas M Vondriska[4], Guangping Li[5], Arjun Deb[8,9], Deepak Srivastava[6,7], Huang-Tian Yang[12–14], Xinshu Xiao[10,11], Hongliang Li[1–3] & Yibin Wang[4,8,9]

Epigenetic reprogramming is a critical process of pathological gene induction during cardiac hypertrophy and remodeling, but the underlying regulatory mechanisms remain to be elucidated. Here we identified a heart-enriched long noncoding (lnc)RNA, named cardiac-hypertrophy-associated epigenetic regulator (*Chaer*), which is necessary for the development of cardiac hypertrophy. Mechanistically, *Chaer* directly interacts with the catalytic subunit of polycomb repressor complex 2 (PRC2). This interaction, which is mediated by a 66-mer motif in *Chaer*, interferes with PRC2 targeting to genomic loci, thereby inhibiting histone H3 lysine 27 methylation at the promoter regions of genes involved in cardiac hypertrophy. The interaction between *Chaer* and PRC2 is transiently induced after hormone or stress stimulation in a process involving mammalian target of rapamycin complex 1, and this interaction is a prerequisite for epigenetic reprogramming and induction of genes involved in hypertrophy. Inhibition of *Chaer* expression in the heart before, but not after, the onset of pressure overload substantially attenuates cardiac hypertrophy and dysfunction. Our study reveals that stress-induced pathological gene activation in the heart requires a previously uncharacterized lncRNA-dependent epigenetic checkpoint.

Cardiac hypertrophy, dysfunction and remodeling are common pathological features in the diseased heart that are driven by transcriptome reprogramming[1–4]. Genome function is highly regulated at the chromatin level by epigenetic modifications; among these, histone lysine methylation is crucial for the recruitment of key protein complexes that regulate genome architecture, genome stability and gene expression[5]. Methylation at histone H3 Lys4 (H3K4) by the trithorax group (TrxG) and mixed-lineage leukemia (MLL) complex is a hallmark of gene activation, whereas methylation at H3 Lys27 (H3K27) by PRC2 leads to gene silencing[6]. Substantial changes in chromatin modifications have been demonstrated in diseased hearts[7–9]. It is clear that pathological reprogramming of the cardiac transcriptome requires a well-orchestrated and stress-signal-dependent regulation of different epigenetic modifications at targeted promoters. However, the underlying molecular mechanisms remain elusive.

Emerging evidence has highlighted important roles for lncRNAs in heart diseases[10–18]. Global transcriptome analyses have identified thousands of lncRNAs whose expression is de-regulated during heart development and pathogenesis, yet few of these have been well studied[19–23]. A number of lncRNAs, termed Epi-lncRNAs[24], are involved in epigenetic regulation by directly interacting with epigenetic modifiers[21,25–27]. *HOX* transcript antisense RNA (*Hotair*) binds to PRC2 and promotes H3K27 trimethylation (H3K27me3) at the promoter region of target genes[25,28]. *Hotair* also binds to lysine-specific demethylase 1A (KDM1A; also known as LSD1) and suppresses histone H3K4 methylation[29]. Two recently identified cardiac-specific lncRNAs, FOXF1-adjacent noncoding developmental regulatory RNA (*Fendrr*) and braveheart long noncoding RNA (*Bvht*), have important roles in cardiac lineage commitment through their interaction with PRC2 (refs. 21,26). Moreover, myosin heavy-chain-associated RNA transcript (*Mhrt*) controls cardiac hypertrophy via targeting SWI–SNF-related, matrix-associated, actin-dependent regulator of chromatin, subfamily a, member 4 (SMARCA4; also known as BRG1)-mediated chromatin modification[30], and *H19* has been reported to function

[1]Department of Cardiology, Renmin Hospital of Wuhan University, Wuhan, China. [2]Animal Experiment Center–Animal Biosafety Level 3 Laboratory, Wuhan University, Wuhan, China. [3]Medical Research Institute, School of Medicine, Wuhan University, Wuhan, China. [4]Division of Molecular Medicine, Department of Anesthesiology, David Geffen School of Medicine, University of California at Los Angeles (UCLA), Los Angeles, California, USA. [5]Department of Cardiology, Tianjin Institute of Cardiology, Second Hospital of Tianjin Medical University, Tianjin, China. [6]Gladstone Institute of Cardiovascular Diseases, San Francisco, California, USA. [7]University of California, San Francisco, School of Medicine, San Francisco, California, USA. [8]Department of Medicine, Cardiology Division, David Geffen School of Medicine, University of California at Los Angeles, Los Angeles, California, USA. [9]Cardiovascular Research Laboratories, David Geffen School of Medicine, University of California at Los Angeles, Los Angeles, California, USA. [10]Department of Integrative Biology and Physiology, College of Life Sciences, Molecular Biology Institute, David Geffen School of Medicine, University of California at Los Angeles, Los Angeles, California, USA. [11]Bioinformatics Interdepartmental Program, University of California at Los Angeles, Los Angeles, California, USA. [12]Key Laboratory of Stem Cell Biology, Institute of Health Sciences, Shanghai Institutes for Biological Sciences, Chinese Academy of Sciences, Shanghai, China. [13]Laboratory of Molecular Cardiology, Institute of Health Sciences, Shanghai Institutes for Biological Sciences, Chinese Academy of Sciences, Shanghai, China. [14]Shanghai Jiao Tong University School of Medicine, Shanghai, China. Correspondence should be addressed to Y.W. (yibinwang@mednet.ucla.edu) or H.L. (lihl@whu.edu.cn).

Received 13 January; accepted 5 August; published online 12 September 2016; doi:10.1038/nm.4179

both as a sponge for the *let-7* family of microRNAs during muscle differentiation[31] and as a modifier of histone H3 methylation during embryonic development[32]. These results implicate divergent functions of lncRNAs in different pathophysiological settings to coordinate epigenetic reprogramming in the heart.

Here we identify a cardiac-enriched lncRNA, *Chaer*, which is both necessary and sufficient for cardiac hypertrophy and induction of genes involved in hypertrophy (hereafter referred to as hypertrophic gene expression), through its interaction with the enhancer of zeste homolog 2 (EZH2) subunit of PRC2.

RESULTS

The lncRNA *Chaer* is necessary for cardiac hypertrophy

From the transcriptomic analysis of pressure-overload-induced failing hearts in mice, we identified nearly 150 lncRNAs that are significantly de-regulated[22]. One of these lncRNAs is a 2,737-nt transcript derived from a two-exon gene located on chromosome 5 of the mouse genome that shows highly enriched expression in heart (**Fig. 1a**,**b**). Moreover, its expression was progressively decreased in the failing heart after transaortic constriction (TAC) surgery (**Supplementary Fig. 1a**). Based on its function, as studied below, we named this lncRNA cardiac-hypertrophy-associated epigenetic regulator (*Chaer*). Translational analysis failed to find any major open-reading frames (ORFs) with translational propensity (**Fig. 1a**, bottom). By using an *in vitro* translation assay in the presence of puromycin, we confirmed that, similarly to *Hotair*, no significant translation events could be detected for *Chaer* RNA (**Fig. 1c**). In addition, none of the predicted small peptides that could potentially be derived from the putative small ORFs in *Chaer* transcript were detected in the mass spectrum data set from PFAM 27.0 (ref. 33). Northern blot analysis identified conserved *Chaer* transcripts in mouse, rat and human hearts as a single band (2.7 kb for mouse and rat *Chaer*; ~2 kb for its human homolog; **Supplementary Fig. 1b–d**). Expression analysis in primary cardiomyocytes and fibroblasts isolated from mouse hearts showed that *Chaer* was specifically expressed in cardiomyocytes but not in fibroblasts (**Supplementary Fig. 1e**). A subcellular fractionation assay detected *Chaer* predominantly in the nuclear fraction, similar to the localization pattern observed for *Hotair* (**Supplementary Fig. 1f**). This subcellular localization was further supported by imaging *Chaer* RNA with fluorescent *in situ* hybridization (FISH) in mouse heart tissue (**Supplementary Fig. 2**).

To determine the functional role of *Chaer*, we used a CRISPR–Cas9-mediated genome-editing approach to inactivate *Chaer* in C57BL/6 mice by deleting exon 2, which contains the majority of the transcript (**Fig. 1d**). Genomic deletion and loss of the *Chaer* transcript in the heart from the knockout (*Chaer*-KO) mice was validated by genomic DNA PCR (**Fig. 1e**) and northern blot analysis (**Supplementary Fig. 1b**). Under basal conditions, we did not observe any morphological or functional phenotype in *Chaer*-KO hearts on the basis of histology, echocardiography and marker gene expression (**Fig. 1f–j**). However, cardiac hypertrophy in response to pressure overload following TAC surgery was significantly attenuated in *Chaer*-KO mice (**Fig. 1f**,**g**). Moreover, pathological fibrosis after TAC was significantly blunted in *Chaer*-KO hearts (**Fig. 1h**,**i**), and cardiac function was preserved (**Fig. 1j**, **Supplementary Fig. 3** and **Supplementary Table 1**).

To further study how *Chaer* contributes to cardiac hypertrophy, we used a *Chaer*-specific siRNA (siChaer) to achieve ~70% knockdown of its expression in isolated neonatal rat ventricular myocytes (NRVMs). *Chaer* knockdown did not change myocyte morphology under basal conditions, but it significantly suppressed hypertrophic growth induced by phenylephrine (PE, 50 μM; **Fig. 2a** and **Supplementary Fig. 4a**). In contrast, NRVMs with *Chaer* overexpression showed a significantly enlarged cell size as compared to that of control cells (**Fig. 2b** and **Supplementary Fig. 4b**). PE induction of hypertrophic gene expression, including that for natriuretic peptide type A (*Nppa*, also known as *Anf*), β-myosin heavy chain (*Myh7*) and skeletal muscle α-actin (*Acta1*), was markedly attenuated after *Chaer* knockdown (**Supplementary Fig. 4c**), whereas *Chaer* overexpression substantially increased their expression in the absence of PE stimulation, except that the effect for *Anf* did not reach significance (**Supplementary Fig. 4d**). In addition, expression of the gene neighboring *Chaer*, HOP homeobox (*Hopx*), was not affected by *Chaer* inactivation or overexpression, suggesting that *Chaer* functions independently of a *Hopx*-mediated *cis* mechanism (**Supplementary Fig. 4c**,**d**). These *in vivo* and *in vitro* data indicate that *Chaer* is necessary and sufficient for cardiomyocyte hypertrophy and pathological gene expression.

Chaer negatively regulates PRC2 function during hypertrophy

To investigate the molecular mechanisms underlying *Chaer* function in cardiomyocytes, we performed RNA sequencing (RNA-seq) analysis in cardiomyocytes with or without *Chaer* knockdown under basal and hypertrophic stimulation. Clustering analysis revealed that for 48.3% of the genes whose expression was changed by PE treatment (>1.5-fold), the effect of PE treatment was markedly reversed by *Chaer* knockdown (**Supplementary Fig. 5a** (left),**5b** (top)); moreover, for 68.8% of the genes whose expression was affected by *Chaer* deficiency (>1.5-fold), their expression was oppositely regulated by PE treatment (**Supplementary Fig. 5a** (right),**5b** (bottom)). Cardiomyopathy-related and cell-cycle-related genes were enriched in the genes whose expression was negatively correlated between the conditions of *Chaer* deficiency and PE treatment (**Supplementary Tables 2** and **3**). This observation suggests a broad effect of *Chaer*-mediated regulation on transcriptome reprogramming during hypertrophy. Notably, 27 of the top 50 downregulated genes following *Chaer* knockdown were clustered in 11 genomic loci (**Supplementary Table 4**), including the imprinted gene *H19* (**Supplementary Fig. 5c–e**), implicating *Chaer*-mediated chromatin remodeling in transcriptome reprogramming. Histone methylation has been implicated in transcriptome reprogramming during cardiac hypertrophy and heart failure[7–9]. Indeed, we observed a dynamic change in global histone methylation at H3K9 and H3K27 sites, but not at H3K4 sites, following PE treatment in NRVMs (**Supplementary Fig. 5f**). *Chaer* deficiency in cardiomyocytes specifically increased di- and trimethylation at H3K27 without affecting the levels of dimethylation at H3K4 (H3K4me2) or H3K9 (H3K9me2) sites (**Fig. 2c**), whereas *Chaer* overexpression specifically reduced H3K27 trimethylation without detectable effect on other types of histone methylation (**Fig. 2d**). These data imply a specific and negative regulation of H3K27 methylation by *Chaer* in cardiomyocytes.

Di- and trimethylation at H3K27 are catalyzed by the histone methyltransferase PRC2, which is a well-known molecular target of several regulatory lncRNAs[25,34]. Using an RNA immunoprecipitation (RIP) assay, we detected a dramatic enrichment of *Chaer* in immunoprecipiates with the PRC2 components SUZ12 and EZH2, but not with the TrxG–MLL components WDR5 or LSD1. As a control, *Hotair* was detected to interact with both PRC2 and LSD1, as previously reported[29] (**Fig. 2e**). Of note, *Chaer* knockdown in cardiomyocytes markedly augmented the interaction between PRC2 and *Hotair* or *Fendrr*[21] without changing the total expression levels of these lncRNAs (**Supplementary Fig. 6a**,**b**). Conversely, *Chaer* overexpression in

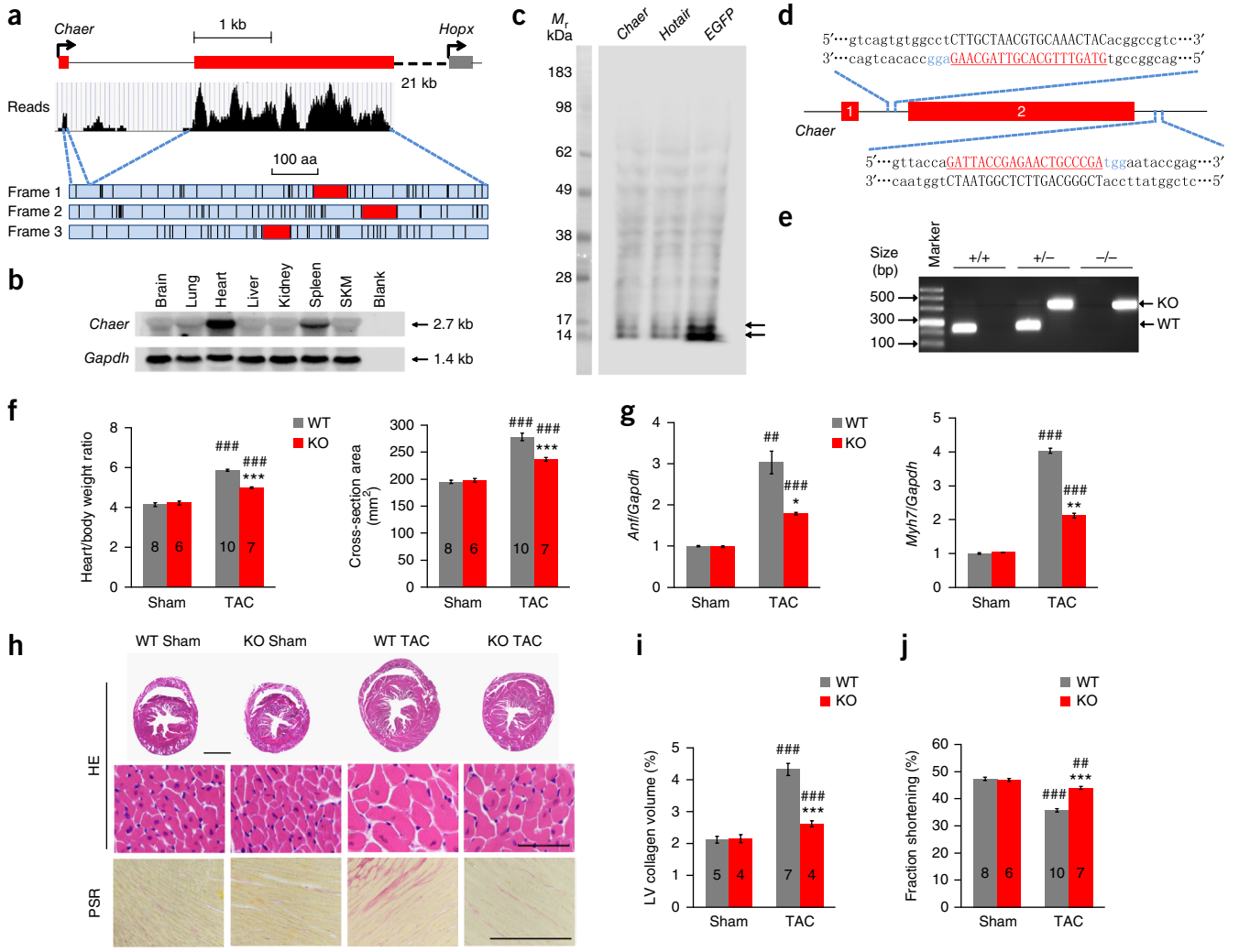

Figure 1 *Chaer* regulates cardiac hypertrophy. (**a**) Genomic structure of the mouse *Chaer* locus (top); the read coverage from RNA sequencing data for mouse *Chaer* (middle); and schematic showing potential ORFs in the three reading frames of mouse *Chaer* (bottom)—stop codons are indicated by vertical black lines, and the longest ORFs are labeled in red. (**b**) Northern blot analysis of *Chaer* in adult mouse tissues. Glyceraldehyde 3-phosphate dehydrogenase (*Gapdh*) was used as a loading control. SKM, skeletal muscle. (**c**) Representative western blot (of $n = 2$) for puromycin incorporation into proteins in an *in vitro* translation assay using *Chaer*, *Hotair* and *EGFP* RNAs. (**d**) Schematic of the *Chaer*-knockout allele in the mouse genome, generated using the CRISPR–Cas9 system. Shown are the two exons (1 and 2) of *Chaer*, the two guide RNA sequences (in red) and an adjacent protospacer motif signal (in blue) that flanked exon 2 of *Chaer*. (**e**) Representative agarose gel electrophoresis analysis for wild-type (WT) and knockout (KO) alleles of *Chaer*, as detected by genomic DNA PCR in WT (+/+), *Chaer*-heterozygous KO (+/–) and *Chaer*-homozygous KO (–/–) mice. The analysis was performed for every mouse used in this study. (**f**) Effect of *Chaer* KO on the heart/body weight ratio (left) and on the cross-sectional area of myocytes (right) 4 weeks after TAC surgery. The numbers of mice tested for each group are indicated in the respective bars. Data are mean ± s.e.m. $^{***}P < 0.001$ (versus WT); $^{###}P < 0.001$ (versus sham); by Student's *t*-test. (**g**) Effect of *Chaer* KO on the expression of *Anf* (left) and *Myh7* (right) 4 weeks after TAC surgery ($n = 3$ mice per group). Data are mean ± s.e.m. $^{*}P < 0.05$ and $^{**}P < 0.01$ (versus WT); $^{##}P < 0.01$, $^{###}P < 0.001$ (versus sham); by Student's *t*-test. (**h**) Representative low- (top) and high-magnification (middle) H&E-stained images and PicroSirius Red (PSR)-stained images (bottom) of WT or *Chaer*-KO hearts 4 weeks after sham or TAC surgery (the numbers of mice tested are indicated in **i**). Scale bars, 2 mm (top), 50 μm (middle and bottom). (**i**,**j**) Left ventricular (LV) collagen volume (**i**) and fractional shortening (**j**). The numbers of mice tested are indicated in the bars. Data are mean ± s.e.m. $^{***}P < 0.001$ (versus WT); $^{##}P < 0.01$ and $^{###}P < 0.001$ (versus sham); by Student's *t*-test.

mouse embryonic fibroblasts (MEFs), in which no endogenous *Chaer* was expressed, markedly reduced the interaction of *Hotair* or *Fendrr* with PRC2, even though the total expression levels of these lncRNAs were increased (**Supplementary Fig. 6c**,**d**). To further demonstrate the functional effect of the *Chaer*–PRC2 interaction, we examined the effect of *Chaer* on *H19* expression, a well-established target whose expression is suppressed by a lncRNA–PRC2 complex. In contrast to the inhibitory effect of *Hotair*, *Chaer* expression markedly induced *H19* expression in MEFs, whereas overexpression of *Hotair* competed with and blocked *Chaer*-induced *H19* expression (**Supplementary Fig. 6e**). Taken together, these data suggest that the interaction of *Chaer* with PRC2 antagonizes PRC2 binding to other lncRNAs and relieves the suppressive function of PRC2 on target genes, an effect distinct from other known PRC2-binding lncRNAs.

The molecular basis of *Chaer*-mediated PRC2 regulation

To further characterize the *Chaer*–PRC2 interaction at a molecular level, we conjugated a modified streptavidin-binding S1 RNA

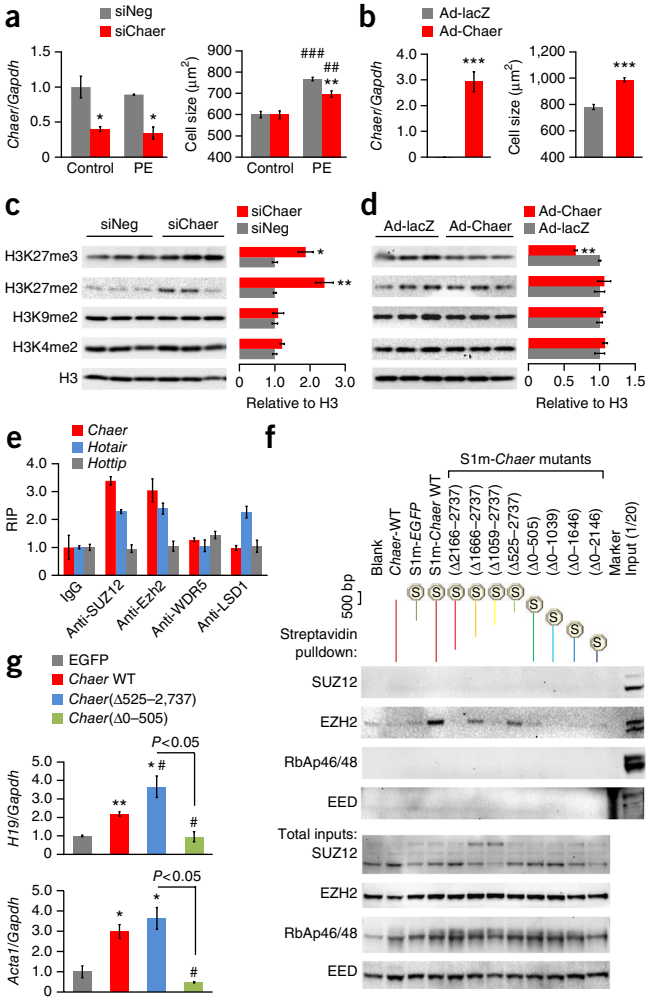

Figure 2 *Chaer* negatively regulates H3K27 trimethylation via its interaction with the catalytic subunit of PRC2. (**a**) *Chaer* expression in (left), and cell size of (right), control and PE-treated (50 μM) NRVMs with (siChaer) or without (siNeg; negative control siRNA) *Chaer* knockdown ($n = 3$ biological replicates)). Data are mean ± s.e.m. $^{*}P < 0.05$ and $^{**}P < 0.01$ (versus siNeg); $^{\#\#}P < 0.01$ and $^{\#\#\#}P < 0.001$ (versus control); by Student's *t*-test. (**b**) *Chaer* expression in (left), and cell size of (right), NRVMs following infection with a control adenovirus (Ad-lacZ) or one overexpressing *Chaer* (Ad-Chaer) ($n = 3$ biological replicates). Data are mean ± s.e.m. $^{***}P < 0.001$ by Student's *t*-test. (**c**,**d**) Representative western blot analyses (left) and quantification of H3 methylation (right), as indicated, in NRVMs in which *Chaer* was knocked down (**c**) or overexpressed (**d**) ($n = 3$ biological replicates). Methylated H3 levels were normalized to total H3 levels. Data are mean ± s.e.m. $^{*}P < 0.05$ and $^{**}P < 0.01$; by Student's *t*-test (versus siNeg (**c**) or Ad-lacZ (**d**) controls). (**e**) RNA immunoprecipitation (RIP) analysis using the antibodies indicated, followed by qRT–PCR for *Chaer*, *Hotair* and *Hoxa* distal transcript antisense RNA (*Hottip*). Values were normalized to the corresponding normal IgG RIP groups. Data are mean ± s.d. from triplicates with one repeat. (**f**) Representative western blot analysis (of $n = 2$) of a tagged-RNA streptavidin pulldown assay. Full-length (WT) *Chaer* and truncated *Chaer* mutants, as indicated, were tagged with a modified S1 motif (S1m) and transfected into MEFs for 48 h, followed by streptavidin-bead pulldown. PRC2 components including SUZ12, EZH2, retinoblastoma-associated proteins 46 and 48 (RbAp46/48) and embryonic ectoderm development (EED) were detected by immunoblotting in the pulldown products (top set) and total inputs (bottom set). (**g**) *H19* (top) and *Acta1* (bottom) expression, as determined by qRT–PCR, in MEFs expressing *EGFP*, WT *Chaer* or either of two *Chaer* fragments (*Chaer*(Δ525–2,737 or *Chaer* (Δ0–505)) ($n = 3$ biological replicates). Data are mean ± s.e.m. $^{*}P < 0.05$ and $^{**}P < 0.01$ (versus *EGFP*); $^{\#}P < 0.05$ (versus *Chaer* WT); by Student's *t*-test.

tag (S1m)[35] with full-length or truncated fragments of *Chaer* (**Supplementary Fig. 7**). All constructs were expressed in MEFs at similar levels (**Supplementary Fig. 7**). We then used streptavidin-conjugated beads in protein pulldown experiments. As compared to the negative controls (including the blank, untagged wild-type (WT) *Chaer* and tagged EGFP), tagged full-length *Chaer* specifically pulled down EZH2 but not the SUZ12, RbAp46, RbAp48 or EED components of the PRC2 complex (**Fig. 2f**). On the basis of the results with the truncated fragments, several regions in *Chaer* (including nt 2,166–2,737 and nt 1,059–1,666) were identified to be necessary for its interaction with EZH2. However, only one 524-nt region (*Chaer*(Δ525–2737)) near the 5′ end of *Chaer* was found to be both necessary and sufficient for EZH2 binding (**Fig. 2f**). Expression of this fragment alone was sufficient to increase the expression of *H19* and the muscle-specific gene *Acta1* in MEFs to the same levels as did expression of full-length *Chaer*, whereas expression of a similar-sized fragment of *Chaer* without the EZH2-binding region (*Chaer*(Δ0–505)) showed no effect (**Fig. 2g**).

Within the 5′ 524-nt fragment, we identified a 66-nt motif with a predicted secondary structure of two connected stem–loops, with four nucleotides in each loop (termed a bi-tetra-loop), similar to a previously validated 89-mer EZH2–EED-interacting motif in *Hotair*[36], and a 56-mer motif found in *Fendrr*. The secondary structure of this motif is conserved among mouse, rat and human *Chaer* homologs (**Fig. 3a** and **Supplementary Fig. 8a–c**). Several differences in the sequences of the predicted stem structures are present between the mouse and rat homologs; however, these differences are paired and do not affect the predicted stem structures (**Fig. 3a**). To demonstrate the direct interaction between this motif and PRC2, we performed an RNA electrophoresis mobility shift assay (EMSA) and detected a specific complex between the *Chaer* 66-mer and recombinant EZH2 (**Fig. 3b**). This interaction was effectively competed by the EZH2-binding motifs from either *Chaer* or *Hotair*, supporting the notion of a similar binding interaction for these two lncRNAs (**Fig. 3b**). However, the EZH2-binding motif from *Chaer* showed lower binding affinity than the motif from *Hotair* (**Fig. 3c**). Moreover, a binding-propensity analysis revealed a similar predicted interaction pattern in the EZH2 RNA-binding region of *Chaer* and *Hotair* (**Fig. 3d** and **Supplementary Fig. 8d**). These data suggest that *Chaer* possesses a potential EZH2-binding motif with shared features to the PRC2-binding motif in *Hotair*.

Regulation of the *Chaer*–PRC2 interaction by hypertrophic signals

Although *Chaer* negatively regulates PRC2 function through a direct interaction in cells, it did not directly affect the enzymatic activity of PRC2 *in vitro* (**Fig. 4a**). However, a chromatin immunoprecipitation (ChIP) assay with an EZH2-specific antibody revealed that *Chaer* overexpression in MEFs led to reduced binding of PRC2 to the *H19* promoter (**Supplementary Fig. 9a**), suggesting that *Chaer* affects PRC2-mediated epigenetic modification by altering its binding at specific gene loci. In support of the concept that *Chaer* regulates PRC2 function during cardiac hypertrophy, RIP analysis with anti-EZH2 and anti-SUZ12 detected a transient but robust enhancement of *Chaer*–PRC2 interaction in NRVMs within the first 8 h of PE treatment, which was inversely correlated with the *Hotair*–PRC2 interaction profile (**Fig. 4b**). This early transient interaction preceded a progressive decrease of global H3K27me3 levels (**Supplementary Fig. 9b**), followed by induction of hypertrophic gene expression (**Supplementary Fig. 9c**). Notably, pre-emptive inactivation of *Chaer*

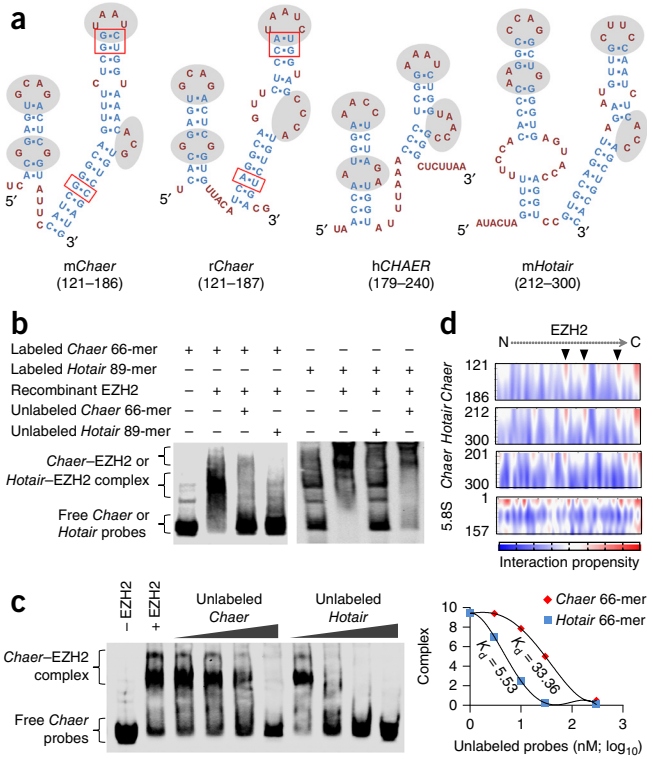

Figure 3 Characterization of a *Chaer* motif that interacts with PRC2. (**a**) Predicted secondary structures of a 66-mer motif in mouse (m)*Chaer*, a 67-mer motif in rat (r)*Chaer*, a 62-mer motif in human (h)*CHAER* and an 89-mer motif in mouse (m)*Hotair*. The unpaired loops with similar patterns are highlighted with a gray background, and sequence differences in the stems between mouse and rat *Chaer* are highlighted with red boxes. (**b**) Representative RNA EMSA analysis for detection of *Chaer*–EZH2 and *Hotair*–EZH2 complexes. Recombinant EZH2 was incubated with labeled m*Chaer* motif or m*Hotair* motif, with or without unlabeled m*Chaer* motif or m*Hotair* motif. (**c**) Left, detection of the *Chaer*–Ezh2 complex using RNA EMSA. Labeled *mChaer* was incubated with increasing concentrations of unlabeled m*Chaer* or m*Hotair* with (+ EZH2) or without (–EZH2) addition of recombinant EZH2 complex. Right, binding profile and dissociation constants were calculated as the concentration of unlabeled *Chaer* or *Hotair* that was needed to cause 50% dissociation of the EZH2–*Chaer* complex. The *y* axis represents the relative amount the *Chaer*–Ezh2 or *Hotair*–Ezh2 complexes, as determined by densitometry, in arbitrary units. (**d**) Interaction propensity for full-length EZH2 binding, depicted from the N to the C terminus of EZH2, with the *Chaer* 66-mer motif, the *Hotair* 89-mer motif, the *Chaer* 201–300-nt fragment and 5.8S rRNA, as predicted by CatRAPID. The arrowheads highlight the predicted RNA-binding sites of EZH2. The *y* axis represents the RNA sequence locations from the corresponding transcripts. Color bar indicates the predicted interaction propensity from low (blue) to high (red).

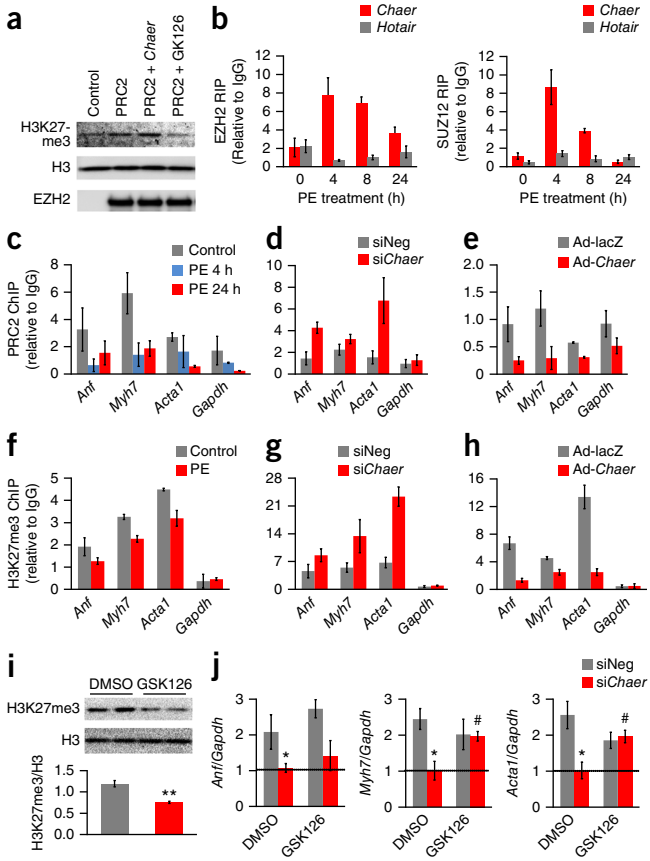

Figure 4 Transiently enhanced *Chaer*–PRC2 interaction regulates hypertrophic gene induction and targeted H3K27me3 modification. (**a**) Methyl transferase activity, as assessed by immunoblotting using anti-H3K27me3 antibody, for recombinant PRC2 complex in the presence or absence of *Chaer* and the EZH2 inhibitor GSK126, using recombinant histone H3 as the substrate ($n = 3$ biological replicates). (**b**) Time-dependent effects of PE treatment on *Chaer*–PRC2 and *Hotair*–PRC2 interactions, as assessed by RIP assays using antibodies to EZH2 (left) or SUZ12 (right). Data are mean ± s.d. from triplicates, performed twice. (**c**–**e**) Chromatin immunoprecipitation (ChIP) analysis, using anti-EZH2, for the promoter regions of *Anf*, *Myh7* and *Acta1* in NRVMs with or without PE treatment for 4 or 24 h (**c**), in PE-treated NRVMs transfected with siNeg or si*Chaer* (**d**), and in NRVMs expressing lacZ (Ad-lacZ) or *Chaer* (Ad-*Chaer*) (**e**). Data are mean ± s.d. from triplicates, and experiments were performed twice. (**f**–**h**) ChIP analysis with anti-H3K27me3 for the promoter regions of *Anf*, *Myh7* and *Acta1* in NRVMs with or without PE treatment (**f**), in PE-treated NRVMs transfected with siNeg or si*Chaer* (**g**), and in NRVMs expressing lacZ (Ad-lacZ) or *Chaer* (Ad-*Chaer*) (**h**). Data are mean ± s.d. from triplicates, performed twice. In **c**–**h**, *Gapdh* expression was used as a control. (**i**) Representative immunoblot analysis (top) and quantification (bottom) for global H3K27me3 levels in NRVMs with or without (DMSO) treatment with the EZH2 inhibitor GSK126 (1 μM) ($n = 3$ biological replicates). Data are mean ± s.e.m. $^{**}P < 0.01$ by Student's *t*-test. (**j**) Effects of GSK126 treatment on *Anf* (left), *Myh7* (middle) and *Acta1* (right) expression, relative to that of *Gapdh*, in PE-treated NRVMs with (siChaer) or without (siNeg) *Chaer* knockdown ($n = 3$ biological replicates). Expression of the genes under basal (siNeg-expressing, DMSO-treated) conditions is indicated by a horizontal line. Data are mean ± s.e.m. $^{*}P < 0.05$ (versus siNeg); $^{\#}P < 0.05$ (versus DMSO); by Student's *t*-test.

expression substantially blocked the PE-induced reduction in global H3K27me3 levels in cardiomyocytes (**Supplementary Fig. 9d**). Consistent with our observations in MEFs, PRC2 ChIP analysis in NRVMs showed that PE treatment decreased PRC2 binding to the promoter regions of the hypertrophic genes *Anf*, *Myh7* and *Acta1* (**Fig. 4c**); moreover, this effect was reversed by *Chaer* inactivation (**Fig. 4d**). Overexpression of *Chaer* in NRVMs was sufficient to reduce PRC2 targeting to these genes (**Fig. 4e**). *Chaer* knockdown reversed the PE-triggered reduction of H3K27me3 levels at the hypertrophic genes (**Fig. 4f**,**g**), whereas *Chaer* overexpression substantially decreased H3K27me3 levels (**Fig. 4h**). Finally, to demonstrate that *Chaer*-mediated gene regulation was dependent on PRC2 activity, we tested the effect of the EZH2 inhibitor GSK126 (1 μM) in PE-treated NRVMs (**Fig. 4i**). Indeed, PRC2 inhibition abolished the effect of *Chaer* knockdown on hypertrophic gene expression (significant for *Myh7* and *Acta1*, and a trend for *Anf*) in PE-treated NRVMs (**Fig. 4j**).

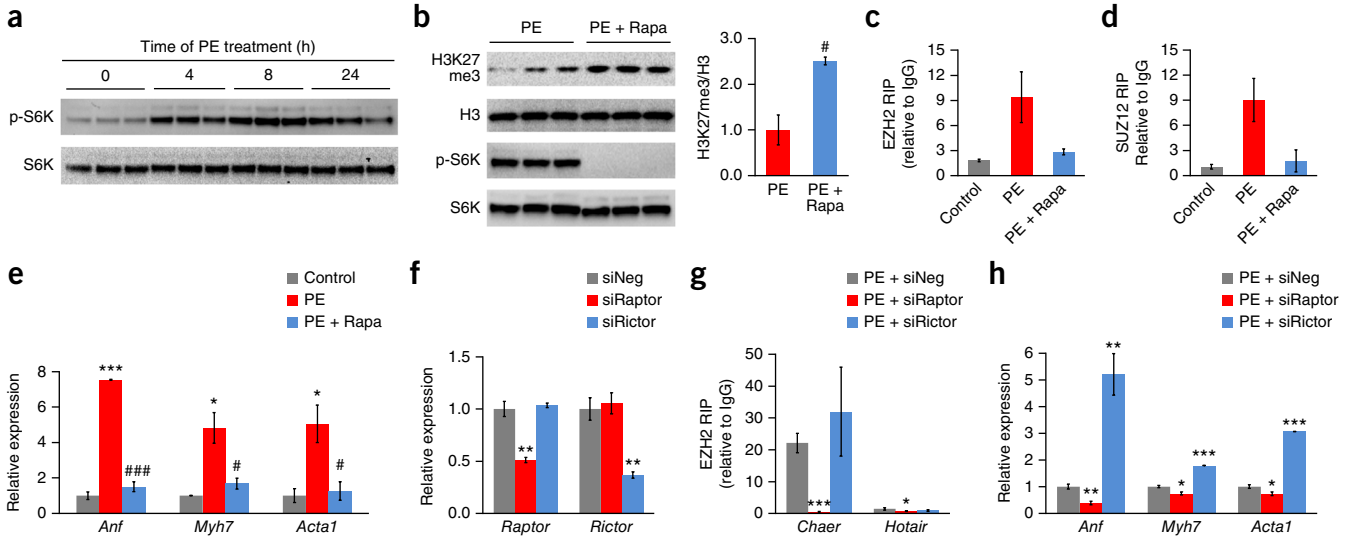

Figure 5 mTORC1 signaling pathway mediates the EZH2–*Chaer* interaction after hypertrophic stimulation. (**a**) Immunoblotting analysis for total and phosphorylated ribosomal protein S6 kinase (S6K) in NRVMs that were treated with PE for the indicated times ($n = 3$ biological replicates). (**b**) Immunoblotting analysis (left) for H3K27me3, total H3, and total and phosphorylated S6K, and quantification of H3K27me3 levels, relative to total H3 levels, (right) in NRVMs treated with PE only or with PE and the mTOR inhibitor rapamycin (Rapa, 20 nM) ($n = 3$). Quantitative data are mean ± s.e.m. $^{\#}P < 0.01$ by Student's *t*-test. (**c**,**d**) RIP analysis of the *Chaer*–PRC2 interaction using anti-EZH2 (**c**) or anti-SUZ12 (**d**) in untreated (control) or PE-treated (4 h) NRVMs, with or without rapamycin treatment. Data are mean ± s.d. from triplicates; the experiment was performed twice. (**e**) qRT–PCR analysis for *Anf*, *Myh7* and *Acta1* expression in untreated or PE-treated (4 h) NRVMs, with or without rapamycin treatment ($n = 3$). Data are mean ± s.e.m. $^{*}P < 0.05$ and $^{***}P < 0.001$ (versus control); $^{\#}P < 0.05$ and $^{\#\#\#}P < 0.001$ (versus PE only treatment); by Student's *t*-test. (**f**) RT–PCR validation of siRNA-mediated knockdown of *Raptor* and *Rictor* ($n = 3$). Data are mean ± s.e.m. $^{**}P < 0.01$ versus siNeg by Student's *t*-test. (**g**) RIP analysis of the *Chaer*–PRC2 and *Hotair*–PRC2 interactions using an EZH2-specific antibody in PE-treated NRVMs that were transfected with siNeg, siRaptor or siRictor. Data are mean ± s.d. from triplicates. (**h**) qRT–PCR analysis for *Anf*, *Myh7* and *Acta1* expression in PE-treated NRVMs that were transfected with siNeg, siRaptor or siRictor ($n = 3$). Data are mean ± s.e.m. $^{*}P < 0.05$, $^{**}P < 0.001$, $^{***}P < 0.001$; versus siNeg; by Student's *t*-test.

These data establish that a transiently enhanced interaction between *Chaer* and PRC2 at the onset of hypertrophic stimulation in cardiomyocytes is both necessary and sufficient to release pathological gene suppression by H3K27 trimethylation.

The transient interaction between *Chaer* and the PRC2 complex after hypertrophic stimulation indicates that a dynamic signaling cascade is involved in this process. Concurrent with the enhanced *Chaer*–PRC2 interaction, the mTOR signaling pathway, as assessed by downstream ribosomal protein S6 kinase (S6K) phosphorylation[37], was rapidly activated following PE treatment in NRVMs (**Fig. 5a** and **Supplementary Fig. 10a**). Indeed, mTOR inhibition by either rapamycin (**Fig. 5b**) or amino acid starvation[38] (**Supplementary Fig. 10b**) completely blocked the PE-induced enhancement of the *Chaer*–PRC2 interaction (**Fig. 5c**,**d** and **Supplementary Fig. 10c**). Conversely, re-feeding of the amino-acid-starved NRVMs dramatically enhanced the *Chaer*–PRC2 interaction in a rapamycin-sensitive manner (**Supplementary Fig. 10d**). Moreover, mTOR inhibition significantly reversed the decrease in global H3K27me3 levels in response to PE treatment (**Fig. 5b**) and suppressed PE-induced hypertrophic gene expression (**Fig. 5e**). These data suggest that the enhancement of the *Chaer*–PRC2 interaction by hypertrophic stimulation is a specific and mTOR-dependent event.

Two distinct mammalian target of rapamycin complexes (mTORCs) exist, namely mTORC1 and mTORC2, which are specified, respectively, by the presence of either regulatory-associated protein of mTOR (Raptor)[39] or rapamycin-insensitive companion of mTOR (Rictor)[40]. To test which complex contributes to the *Chaer*-mediated hypertrophic transition, we knocked down the expression of *Raptor* or *Rictor* in NRVMs using specific siRNAs (**Fig. 5f**). Inactivation of *Raptor*, but not *Rictor*, completely abolished the enhanced *Chaer*–PRC2 interaction after PE treatment (**Fig. 5g**). In line with this observation, PE-induced expression of *Anf*, *Myh7* and *Acta1* was significantly suppressed by *Raptor* knockdown but was even further enhanced by *Rictor* knockdown (**Fig. 5h**). Finally, *Chaer* overexpression partially reversed the effects of rapamycin treatment (**Supplementary Fig. 10e**) and *Raptor* knockdown (**Supplementary Fig. 10f**) in repressing hypertrophic gene expression, suggesting a cross-talk between mTORC1 and the *Chaer*–PRC2 interaction in mediating cardiomyocyte hypertrophic gene expression.

A *Chaer*-mediated epigenetic checkpoint for cardiac hypertrophy

To study the *Chaer*–PRC2 pathway *in vivo*, we further analyzed the effect of *Chaer* inactivation on epigenetic modulation in the mouse heart. After TAC surgery, global H3K27me2 and H3K27me3 levels were significantly increased in hearts from *Chaer*-KO mice (hereafter referred to as *Chaer*-KO hearts), with no significant changes observed for H3K9me2 or H3K9me3 levels (**Fig. 6a**). ChIP analysis showed that H3K27me3 levels at the promoter regions of *Anf*, *Myh7* and *Acta1* were dramatically reduced at 2 weeks after TAC surgery in WT hearts, but were significantly increased in *Chaer*-KO hearts (**Fig. 6b**). Similar to what we observed *in vitro*, the *Chaer*–PRC2 interaction in the heart showed a dramatic but transient enhancement as early as 1 h after TAC surgery, and this began to diminish 4 h later (**Fig. 6c**). To investigate the significance of the early onset of the *Chaer*–PRC2 interaction, we used a nanoparticle-mediated transfection method[41] to deliver a chemically modified siChaer into the heart, which achieved an effective silencing of *Chaer* expression within the experimental time frame (**Supplementary Fig. 11a**). By using two delivery strategies, with siRNA injection before (protocol 1) or after (protocol 2) TAC surgery (**Fig. 6d** and **Supplementary Fig. 11b**,**c**), we observed that pre-emptive *Chaer* knockdown in the

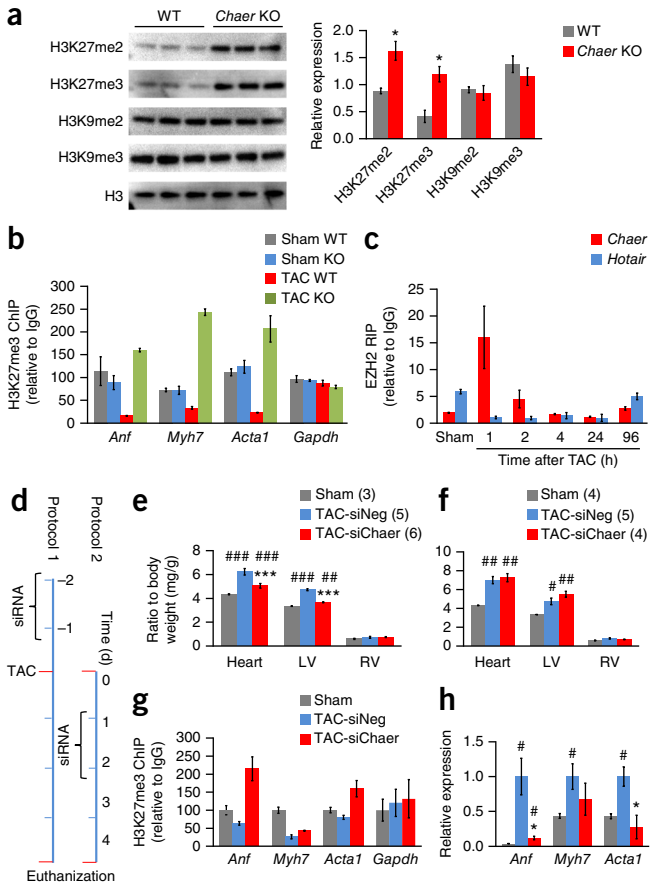

Figure 6 *Chaer* functions as an early checkpoint for TAC-induced hypertrophy *in vivo*. (**a**) Immunoblotting analysis (left) and quantification (right) of H3 modifications, as indicated, in WT and *Chaer*-KO hearts 2 weeks after TAC surgery ($n = 3$ mice per group). Methylated H3 levels were normalized to total H3 levels. Data are mean ± s.e.m. $^{*}P < 0.05$ versus WT by Student's *t*-test. (**b**) ChIP analysis for H3K27me3 levels at the promoter regions of *Anf*, *Myh7*, *Acta1* and *Gapdh* in WT and *Chaer*-KO hearts from mice that underwent either sham or TAC surgery. Data are mean ± s.d. from triplicates from one mouse per group. (**c**) Time course of the *Chaer*–PRC2 interaction, as measured by anti-EZH2 RIP, in a mouse heart after TAC surgery. Data are mean ± s.d. from triplicates from one mouse. (**d**) Schematic of the two protocols for *Chaer* inactivation. Two siRNA injections were performed before (protocol 1) or after (protocol 2) TAC surgery. (**e**,**f**) Effects of *Chaer* knockdown *in vivo* on the weights of the hearts and of the left (LV) and right (RV) ventricles following protocol 1 (**e**) or protocol 2 (**f**) in sham-treated mice or in siRNA-expressing mice that underwent TAC surgery (TAC-siNeg or TAC-si*Chaer*) (the numbers of mice tested in each group are indicated in parentheses). Data are mean ± s.e.m. $^{***}P < 0.001$ (versus siNeg); $^{\#}P < 0.05$, $^{\#\#}P < 0.01$, $^{\#\#\#}P < 0.001$ (versus Sham); by Student's *t*-test. (**g**) ChIP analysis for H3K27me3 levels at the promoter regions of *Anf*, *Myh7*, *Acta1* and *Gapdh* in the hearts from the sham, TAC-siNeg and TAC-si*Chaer* groups mice treated according to protocol 1. Data are mean ± s.d. from triplicates from one mouse. (**h**) qRT–PCR analysis for *Anf*, *Myh7* and *Acta1* expression in the hearts of the sham, TAC-siNeg and TAC-si*Chaer* groups of mice treated according to protocol 1 ($n = 3$ mice per group). Data are mean ± s.e.m. $^{*}P < 0.05$ (versus siNeg); $^{\#}P < 0.05$ (versus Sham); by Student's *t*-test.

heart significantly suppressed cardiac hypertrophy and resulted in preserved cardiac function and decreased fibrotic remodeling (**Fig. 6e**,**f** and **Supplementary Fig. 11d–f**). Moreover, hypertrophic gene expression was also significantly blunted, in line with an attenuated reduction of H3K27me3 levels at their promoter regions (**Fig. 6g**,**h**). These results further support the essential role of the *Chaer*–PRC2 interaction in epigenetic regulation during cardiac hypertrophy. In marked contrast, delivery of the same *Chaer*-specific siRNA 1 d after TAC surgery failed to affect the progression of cardiac hypertrophy, despite a comparable level of *Chaer* silencing (**Fig. 6f** and **Supplementary Fig. 11b**). These data reveal a critical time window immediately following the onset of pathological stress, in which an epigenetic checkpoint controls the progression of cardiac hypertrophy and pathological remodeling.

Chaer–PRC2 interaction and regulation in human cardiomyocytes

Expression of the human *CHAER* transcript was readily detected in human heart (**Supplementary Fig. 1d**). Using two independent pairs of primers, we detected an increase of *CHAER* expression in hearts from individuals with dilated cardiomyopathy, as compared to nondiseased control hearts, although this difference was not significant owing to large variations in *CHAER* levels (**Supplementary Fig. 12a**). To study *CHAER* function in human cardiomyocytes, we first performed RIP analysis using anti-EZH2 in human induced pluripotent stem cell–derived cardiomyocytes (hiPSC-CMs). We found that *CHAER* specifically interacted with EZH2 in a rapamycin-sensitive manner (**Supplementary Fig. 12b**). Next, by using nanoparticle-mediated transfection of human *CHAER* into hiPSC-CMs, we observed that *CHAER* overexpression led to an increased expression of the hypertrophic genes *ANF*, *MYH7* and *ACTA1* (**Supplementary Fig. 12c**,**d**). To test the functional conservation of *Chaer*, we expressed human *CHAER* in rat myocytes (**Supplementary Fig. 12e**). Similar to mouse *Chaer* overexpression, human *CHAER* overexpression in NRVMs increased hypertrophic gene expression (**Supplementary Fig. 12f**). Moreover, overexpression of mouse *Chaer* in NRVMs rescued the suppression on PE-induced expression of hypertrophic genes caused by knockdown of endogenous (rat) *Chaer* (**Supplementary Fig. 12g–i**). Finally, overexpression of either mouse *Chaer* or human *CHAER* in either mouse cells (MEFs) or human cells (HEK293 cells) led to a similar induction of *H19* expression (**Supplementary Fig. 12j–m**). Taken together, these data suggest that *Chaer* has a conserved gene regulatory function across rodent and human species.

DISCUSSION

Similar to protein-coding genes, lncRNAs contribute markedly to tissue-specific responses, at least in part via epigenetic regulation[22,42]. Genome-wide analysis of histone marks has revealed a complex epigenetic landscape that orchestrates gene expression during cardiac hypertrophy[9]. Here we identified a heart-specific lncRNA, *Chaer*, as a critical regulator of cardiac hypertrophy via its direct interaction with PRC2. This finding, along with other recent reports[21,25–27,30], identify a class of epigenetic regulatory lncRNAs (referred to as Epi-LncRNAs) in cardiac gene regulation[24]. Other PRC2-interacting lncRNAs, such as *Fendrr* and *Bvht*, have been shown to be important in epigenetic programming during heart development[21,26]. In contrast, the lncRNA *Myht* regulates cardiac hypertrophy and pathological remodeling through direct interaction with a histone acetylation factor, BRG1 (ref. 30). Therefore, the effects of Epi-LncRNAs on epigenetic regulation may depend on their interaction with specific protein partners during cardiac development and pathogenesis. *Chaer*, a cardiac-enriched lncRNA, has a hypertrophic signaling-dependent interaction with PRC2 and, as shown by genetic evidence, is essential for cardiac pathological hypertrophy and remodeling *in vivo*.

Elucidation of the molecular basis of lncRNA function is a major challenge in the field. The *Chaer* transcript contains a bi-tetra-loop

motif within its 5′ end that is both sufficient and necessary for PRC2 binding. However, the overall structural basis of *Chaer* function remains speculative and needs to be further investigated. Although the predicted structure of the *Chaer* PRC2-binding motif shares features with other established PRC2-binding motifs in several EZH2-binding lncRNAs[36], *Chaer* binding seems to repress, rather than promote, PRC2 function, as demonstrated for both global and promoter-specific H3K27me3 levels. This negative regulation of PRC2 function is consistent with previous reports that *Ezh2* silencing results in cardiac hypertrophy[43,44]. However, *Chaer* binding does not seem to directly repress PRC2 enzymatic activity, as assessed by an *in vitro* assay, but rather probably interferes with PRC2 genomic targeting. Whereas the *Chaer*–PRC2 interaction is only transiently enhanced at the onset of hypertrophy, the effect of this interaction on downstream H3K27me3 levels seems to be long lasting, given that H3K27me3 levels continue to be suppressed even 2 weeks after TAC surgery. Therefore, *Chaer* contributes to the timing and specificity of cardiac epigenetic reprogramming during hypertrophy by targeted modulation of histone methylation and de-methylation at the onset of hypertrophic stimulation[45]. It remains to be determined whether the effects of *Chaer* may also involve other PRC2-binding lncRNAs, such as *Hotair*, or involve other histone modifiers, such as the H3K27-specific histone demethylases UTX and jumonji domain containing 3 (JMJD3)[46].

Despite the well-established involvement of the mTOR pathway in cardiac growth, the role of mTOR in the hypertrophic and failing heart remains elusive[47–52]. One major finding from our study is that the *Chaer*–PRC2 interaction is a stress-induced transient event that depends on mTOR activity. Previously, cyclin-dependent kinase 1 (CDK1)-mediated phosphorylation of EZH2 (at Thr345) has been shown to enhance the binding affinity of EZH2 with lncRNAs, including *Hotair* and *Xist*, during the cell cycle[53]. Although we also observed rapamycin-sensitive EZH2 phosphorylation at Thr345 in PE-treated NRVMs, this phosphorylation occurred at 24 h after PE treatment (data not shown), when the *Chaer*–EZH2 interaction had already passed its peak. Therefore, other mTORC1-dependent modifications of the PRC2 complex may be involved. Considering the sequence diversity in the binding motifs for PRC2 that are found in different lncRNAs, our findings imply that signaling-dependent modulation of PRC2 may dictate its lncRNA binding partners under different physiological and pathophysiological states, leading to tissue-specific and gene-specific epigenetic reprogramming associated with development and disease. Clearly, more studies are needed to dissect the molecular basis of *Chaer*-mediated PRC2 regulation in response to hypertrophic signaling.

Although our study focused on the cell-autonomous effects of *Chaer* on cardiomyocyte hypertrophy, *Chaer* may also have regulatory effects in non-myocyte cardiac cells. Notably, in the FISH assay we detected a substantial signal for *Chaer* within the epicardium, where progenitor cells for endothelial cells and fibroblasts have been reported to reside[54], and *Chaer* KO hearts had significantly reduced TAC-induced cardiac fibrosis. It is also of note that a substantial number of cell-cycle-related genes are regulated by *Chaer*. It remains to be determined whether the broad effect of *Chaer* on cardiac gene expression is mediated through direct effects of epigenetic regulation on gene expression or more indirectly through the secondary effects of master genes under epigenetic regulation.

In summary, our findings reveal a previously uncharacterized epigenetic switch for transcriptome reprogramming at the very beginning of cardiac hypertrophy, involving an mTORC1-dependent interaction between a cardiac-enriched lncRNA, *Chaer*, and the histone modification complex PRC2. This interaction is a prerequisite for hypertrophic gene expression, cardiac hypertrophy and pathological remodeling. Because the *Chaer*–PRC2 interaction is transiently induced immediately following stress stimulation, this interaction is not needed for the progression of hypertrophic remodeling beyond the early epigenetic switch point. Considering the functional conservation between rodent and human *CHAER*, the protective effects of *Chaer* inactivation in the stressed heart suggest that the *Chaer*–PRC2 interaction can serve as a potential therapeutic target in the treatment of cardiac hypertrophy and of pathological remodeling in hypertrophic cardiomyopathy.

METHODS

Methods and any associated references are available in the online version of the paper.

Accession codes. Gene Expression Omnibus: the RNA-seq data are available under accession code GSE82339.

Note: Any Supplementary Information and Source Data files are available in the online version of the paper.

ACKNOWLEDGMENTS

This work was supported in part by the US National Institute of Health (NIH) (grant no. HL070079 (Y.W.), HL103205 (Y.W.), HL108186 (Y.W.), HL110667 (Y.W.), HL115238 (T.M.V.), R01HG006264 (X.X.) and U01HG007013 (X.X.)), the University of California at Los Angeles CTSI–Cardiovascular Pilot Team research grant UL1TR000124 (Y.W., X.X. and T.M.V.), the National Science Fund for Distinguished Young Scholars (grant no. 81425005; H.L.), the Key Project of the National Natural Science Foundation (grant no. 81330005 and 81630011; both to H.L.), the National Science and Technology Support Project (grant no. 2013YQ030923-05, 2014BAI02B01 and 2015BAI08B01; all to H.L.) and an American Heart Association Western States Affiliate Postdoctoral Fellowship (15POST24970034; Z.W.). C.G. was a recipient of the UCLA Eli and Edythe Broad Center Predoctoral Fellowship in Stem Cell Science. H.W. was supported by the China Scholarship Council (award no. 201406280042) and was a recipient of a Jennifer S. Buchwald Graduate Fellowship in Physiology. A.C. was supported by NIH predoctoral training grant T90DE022734. The authors wish to acknowledge outstanding technical support from H. Pu and Core support from the UCLA Cardiovascular Research Laboratories and the Division of Molecular Medicine at UCLA.

AUTHOR CONTRIBUTIONS

Z.W. designed all the experiments with input from H.-T.Y., H.L. and Y.W., performed the majority of the experiments and drafted the manuscript; Y.W. designed and supervised the study; H.L. designed and supervised the *in vivo* experiments; X.-J.Z., Y.-X.J., P.Z. and K.-Q.D. performed the northern blot, ChIP, FISH, immunoblotting and PV loop assays for *Chaer*-KO mice with input from H.L.; K.-Q.D., J.G. and H.L. developed the *Chaer*-knockout mice and performed some of the *in vivo* experiments; X.W. and G.L. participated in the tagged-RNA pulldown assay and RIP assays; I.C., C.G. and H.W. participated in the lncRNA screening and cloning experiments; T.Y. participated in the histology assay; A.C., X.X. and T.M.V. participated in the transcriptome analysis; S.R. performed the TAC surgery; Y.S.A. and D.S. provided the human iPSC-derived cardiomyocytes; S.L. and A.D. provided the primary cardiac fibroblasts and myocytes from mouse heart.

COMPETING FINANCIAL INTERESTS

The authors declare no competing financial interests.

1. Sala, V. *et al.* Signaling to cardiac hypertrophy: insights from human and mouse RASopathies. *Mol. Med.* **18**, 938–947 (2012).
2. Kuwahara, K., Nishikimi, T. & Nakao, K. Transcriptional regulation of the fetal cardiac gene program. *J. Pharmacol. Sci.* **119**, 198–203 (2012).
3. Wang, Y. Mitogen-activated protein kinases in heart development and diseases. *Circulation* **116**, 1413–1423 (2007).
4. Maron, B.J. & Maron, M.S. Hypertrophic cardiomyopathy. *Lancet* **381**, 242–255 (2013).
5. Joh, R.I., Palmieri, C.M., Hill, I.T. & Motamedi, M. Regulation of histone methylation by noncoding RNAs. *Biochim. Biophys. Acta* **1839**, 1385–1394 (2014).

6. Gould, A. Functions of mammalian Polycomb group and trithorax group–related genes. *Curr. Opin. Genet. Dev.* **7**, 488–494 (1997).
7. Kaneda, R. *et al.* Genome-wide histone methylation profile for heart failure. *Genes Cells* **14**, 69–77 (2009).
8. Angrisano, T. *et al.* Epigenetic switch at *Atp2a2* and *Myh7* gene promoters in pressure-overload-induced heart failure. *PLoS One* **9**, e106024 (2014).
9. Papait, R. *et al.* Genome-wide analysis of histone marks identifying an epigenetic signature of promoters and enhancers underlying cardiac hypertrophy. *Proc. Natl. Acad. Sci. USA* **110**, 20164–20169 (2013).
10. Ishii, N. *et al.* Identification of a novel noncoding RNA, *MIAT*, that confers risk of myocardial infarction. *J. Hum. Genet.* **51**, 1087–1099 (2006).
11. Friedrichs, F. *et al. HBEGF*, *SRA1* and *IK*: three co-segregating genes as determinants of cardiomyopathy. *Genome Res.* **19**, 395–403 (2009).
12. Burd, C.E. *et al.* Expression of linear and novel circular forms of an *INK4/ARF*-associated noncoding RNA correlates with atherosclerosis risk. *PLoS Genet.* **6**, e1001233 (2010).
13. Kumarswamy, R. *et al.* Circulating long noncoding RNA, *LIPCAR*, predicts survival in patients with heart failure. *Circ. Res.* **114**, 1569–1575 (2014).
14. Wang, K. *et al.* The long noncoding RNA *CHRF* regulates cardiac hypertrophy by targeting miR-489. *Circ. Res.* **114**, 1377–1388 (2014).
15. Jiang, F., Zhou, X. & Huang, J. Long noncoding RNA–*ROR* mediates the reprogramming in cardiac hypertrophy. *PLoS One* **11**, e0152767 (2016).
16. Viereck, J. *et al.* Long noncoding RNA *Chast* promotes cardiac remodeling. *Sci. Transl. Med.* **8**, 326ra22 (2016).
17. Liu, L. *et al.* The *H19* long noncoding RNA is a novel negative regulator of cardiomyocyte hypertrophy. *Cardiovasc. Res.* **111**, 56–65 (2016).
18. Peters, T. *et al.* Long noncoding RNA *Malat-1* is dispensable during pressure-overload-induced cardiac remodeling and failure in mice. *PLoS One* **11**, e0150236 (2016).
19. Matkovich, S.J., Edwards, J.R., Grossenheider, T.C., de Guzman Strong, C. & Dorn, G.W., II. Epigenetic coordination of embryonic heart transcription by dynamically regulated long noncoding RNAs. *Proc. Natl. Acad. Sci. USA* **111**, 12264–12269 (2014).
20. Ounzain, S. *et al.* Genome-wide profiling of the cardiac transcriptome after myocardial infarction identifies novel heart-specific long noncoding RNAs. *Eur. Heart J.* **36**, 353–68a (2015).
21. Grote, P. *et al.* The tissue-specific lncRNA *Fendrr* is an essential regulator of heart and body wall development in the mouse. *Dev. Cell* **24**, 206–214 (2013).
22. Lee, J.H. *et al.* Analysis of transcriptome complexity through RNA sequencing in normal and failing murine hearts. *Circ. Res.* **109**, 1332–1341 (2011).
23. Kurian, L. *et al.* Identification of novel long noncoding RNAs underlying vertebrate cardiovascular development. *Circulation* **131**, 1278–1290 (2015).
24. Wang, Z. & Wang, Y. Dawn of the Epi-LncRNAs: new path from *Myheart. Circ. Res.* **116**, 235–236 (2015).
25. Li, L. *et al.* Targeted disruption of *Hotair* leads to homeotic transformation and gene de-repression. *Cell Rep.* **5**, 3–12 (2013).
26. Klattenhoff, C.A. *et al. Braveheart*, a long noncoding RNA required for cardiovascular lineage commitment. *Cell* **152**, 570–583 (2013).
27. Wang, K.C. *et al.* A long noncoding RNA maintains active chromatin to coordinate homeotic gene expression. *Nature* **472**, 120–124 (2011).
28. Liu, Z. *et al.* The long noncoding RNA *HOTAIR* contributes to cisplatin resistance of human lung adenocarcinoma cells via downregualtion of p21WAF1/CIP1 expression. *PLoS One* **8**, e77293 (2013).
29. Li, F. *et al.* Characterization of sucrose transporter alleles and their association with seed-yield-related traits in *Brassica napus* L. *BMC Plant Biol.* **11**, 168 (2011).
30. Han, P. *et al.* A long noncoding RNA protects the heart from pathological hypertrophy. *Nature* **514**, 102–106 (2014).
31. Kallen, A.N. *et al.* The imprinted *H19* lncRNA antagonizes *let-7* microRNAs. *Mol. Cell* **52**, 101–112 (2013).
32. Monnier, P. *et al. H19* lncRNA controls gene expression of the Imprinted Gene Network by recruiting MBD1. *Proc. Natl. Acad. Sci. USA* **110**, 20693–20698 (2013).
33. Finn, R.D. *et al.* Pfam: the protein families database. *Nucleic Acids Res.* **42**, D222–D230 (2014).
34. Chu, C., Qu, K., Zhong, F.L., Artandi, S.E. & Chang, H.Y. Genomic maps of long noncoding RNA occupancy reveal principles of RNA–chromatin interactions. *Mol. Cell* **44**, 667–678 (2011).
35. Leppek, K. & Stoecklin, G. An optimized streptavidin-binding RNA aptamer for purification of ribonucleoprotein complexes identifies novel ARE-binding proteins. *Nucleic Acids Res.* **42**, e13 (2014).
36. Wu, L., Murat, P., Matak-Vinkovic, D., Murrell, A. & Balasubramanian, S. Binding interactions between long noncoding RNA *HOTAIR* and PRC2 proteins. *Biochemistry* **52**, 9519–9527 (2013).
37. Kang, S., Chemaly, E.R., Hajjar, R.J. & Lebeche, D. Resistin promotes cardiac hypertrophy via the AMP-activated protein kinase–mammalian target of rapamycin (AMPK–mTOR) and c-Jun N-terminal kinase–insulin receptor substrate 1 (JNK–IRS1) pathways. *J. Biol. Chem.* **286**, 18465–18473 (2011).
38. Sancak, Y. *et al.* The Rag GTPases bind raptor and mediate amino acid signaling to mTORC1. *Science* **320**, 1496–1501 (2008).
39. Kim, D.H. *et al.* mTOR interacts with raptor to form a nutrient-sensitive complex that signals to the cell growth machinery. *Cell* **110**, 163–175 (2002).
40. Sarbassov, D.D. *et al.* Rictor, a novel binding partner of mTOR, defines a rapamycin-insensitive and raptor-independent pathway that regulates the cytoskeleton. *Curr. Biol.* **14**, 1296–1302 (2004).
41. Li, Q., Wang, P., Ye, K. & Cai, H. Central role of SIAH inhibition in DCC-dependent cardioprotection provoked by netrin-1–NO. *Proc. Natl. Acad. Sci. USA* **112**, 899–904 (2015).
42. Cabili, M.N. *et al.* Integrative annotation of human large intergenic noncoding RNAs reveals global properties and specific subclasses. *Genes Dev.* **25**, 1915–1927 (2011).
43. Delgado-Olguín, P. *et al.* Epigenetic repression of cardiac progenitor gene expression by EZH2 is required for postnatal cardiac homeostasis. *Nat. Genet.* **44**, 343–347 (2012).
44. Yang, T. *et al.* MicroRNA-214 provokes cardiac hypertrophy via repression of *EZH2*. *Biochem. Biophys. Res. Commun.* **436**, 578–584 (2013).
45. Shi, L. *et al.* Histone demethylase JMJD2B coordinates H3K4 and H3K9 methylation and promotes hormonally responsive breast carcinogenesis. *Proc. Natl. Acad. Sci. USA* **108**, 7541–7546 (2011).
46. Agger, K. *et al.* UTX and JMJD3 are histone H3K27 demethylases involved in *HOX* gene regulation and development. *Nature* **449**, 731–734 (2007).
47. Song, X. *et al.* mTOR attenuates the inflammatory response in cardiomyocytes and prevents cardiac dysfunction in pathological hypertrophy. *Am. J. Physiol. Cell Physiol.* **299**, C1256–C1266 (2010).
48. Liu, X., Wang, X., Bi, Y., Bu, P. & Zhang, M. The histone demethylase PHF8 represses cardiac hypertrophy upon pressure overload. *Exp. Cell Res.* **335**, 123–134 (2015).
49. Xu, N. *et al.* The alteration of protein prenylation induces cardiomyocyte hypertrophy through Rheb–mTORC1 signaling and leads to chronic heart failure. *J. Pathol.* **235**, 672–685 (2015).
50. Li, Y. *et al.* AMPK inhibits cardiac hypertrophy by promoting autophagy via mTORC1. *Arch. Biochem. Biophys.* **558**, 79–86 (2014).
51. Shende, P. *et al.* Cardiac mTOR complex 2 preserves ventricular function in pressure-overload hypertrophy. *Cardiovasc. Res.* **109**, 103–114 (2016).
52. Shende, P. *et al.* Cardiac Raptor ablation impairs adaptive hypertrophy, alters metabolic gene expression and causes heart failure in mice. *Circulation* **123**, 1073–1082 (2011).
53. Kaneko, S. *et al.* Phosphorylation of the PRC2 component EZH2 is cell-cycle-regulated and upregulates its binding to ncRNA. *Genes Dev.* **24**, 2615–2620 (2010).
54. Marketou, M.E., Parthenakis, F. & Vardas, P.E. Pathological left ventricular hypertrophy and stem cells: current evidence and new perspectives. *Stem Cells Int.* **2016**, 5720758 (2016).

ONLINE METHODS

Animal and human studies. All experimental procedures involving animals in this study were reviewed and approved by the Institutional Animal Care and Use Committees (IACUCs) of University of California at Los Angeles (UCLA) and conformed to the Guide for the Care and Use of Laboratory Animals, published by the US National Institutes of Health[55]. Experiments with donated human heart tissues were approved by the Ethics Committee Board of Wuhan University, China after obtaining proper informed consent. Male, 8- to 10-week-old mice in the C57BL/6 background were used in this study; the number of mice studied in each experiment is indicated. Mice of different genotypes were randomly assigned to the sham or transaortic constriction (TAC) groups. Echocardiographic analysis was performed by an investigator blinded to the genotype or to the procedure (sham or TAC).

Cell culture, plasmids and adenoviral vectors. Neonatal rat ventricular myocytes (NRVMs) were prepared as previously described[56] and maintained in Dulbecco's modified Eagle's medium (DMEM) supplemented with 1% insulin–transferrin–selenium (ITS-G, BD Biosciences, CA, USA), 100 U/mL penicillin and 100 μg/mL streptomycin for 24 h before transfection, infection or drug treatment. Immortalized mouse embryonic fibroblasts (MEFs) and human HEK293 cells, authenticated cell lines from ATCC, were maintained in DMEM supplemented with 10% FBS, 2 mM L-glutamine, 100 U/mL penicillin and 100 μg/mL streptomycin. Human induced pluripotent stem cell–derived cardiomyocytes (hiPSC-CMs) were provided by D.S.'s lab (University of California, San Francisco) and were prepared and maintained as previously reported[57]. Cardiac fibroblasts were obtained from A.D.'s lab (University of California, Los Angeles) and were prepared as previously reported[58]. Cardiomyocytes from adult mouse heart were isolated using enzymatic digestion as described previously[59]. The lack of mycoplasma contamination of MEFs, NRVMs and HEK293 cells was routinely tested using RT–PCR or a commercial kit. Wild-type *Chaer*, truncated *Chaer* mutants and *Hotair* were cloned from mouse cDNA with Turbo Pfu DNA polymerase (Thermo Fisher Scientific, MA, USA) and inserted into the pcDNA5-CMV vector (Thermo Fisher Scientific, MA, USA) for transient overexpression. Human *CHAER* was cloned from donated normal human heart tissues into the pcDNA5-CMV vector and overexpressed in NRVMs with nanoparticle-mediated transfection following the manufacturer's instructions (Altogen). Wild-type *Chaer* and *lacZ* were cloned into pShuttle-CMV and recombined with pAdeasy-1 to generate adenoviruses expressing *Chaer* (Ad-Chaer) and lacZ (Ad-lacZ). *Chaer* 66-mer motif and *Hotair* 89-mer motif were cloned into pBluescript II for *in vitro* transcription. Mouse *Ezh2* was cloned into pT7CFE1 for *in vitro*–coupled transcription and translation. Lipofectamine 2000 (Life Technologies, NY, USA) was used to transfect plasmids into MEFs. Negative-control siRNA (siNeg; CMSINC-30; Bioland Scientific, CA, USA), *Chaer*-specific siRNA (siChaer; 5′-CCCGGACUUAAAUAGUAUAU-3′; designed and synthesized by Bioland Scientific) and *Hotair*-specific siRNA (siHotair; GS10050387; Qiagen, Limburg, the Netherlands) were transfected into NRVMs using Lipofectamine RNAiMAX (Life Technologies). A 1.7-kb-long human *CHAER* homolog was cloned using Zero Blunt TOPO PCR cloning kit (Thermo Fisher Scientific, MA, USA), transferred into pcDNA5-CMV using BamHI and XhoI, and transfected into NRVMs and hiPSC-CMs using nanoparticle-mediated transfection reagents (Altogen Biosystems, NV, USA), according to the manufacturer's instructions. NRVMs or MEFs were infected with Ad-Chaer (10^7 plaque-forming units (PFU)/ml) for overexpression; the same amount of Ad-lacZ was used as a control. Phenylephrine (PE, 50 μM) was used to induce hypertrophy in NRVMs. NRVM starvation was performed by incubating the cells in branched-chain amino acid–depletion medium (Thermo Fisher Scientific) overnight, followed by re-feeding with normal culture medium.

Generation of *Chaer*-knockout mice. *Chaer*-knockout mice were generated using a CRISPR genome-editing system in the C57BL/6 background as previously reported[60]. A pair of single guide RNAs (sgRNAs) flanking exon 2 of *Chaer* (the majority of the lncRNA) was designed using an online CRISPR design tool (http://tools.genome-engineering.org) and inserted into the vector pUC57-sgRNA (Addgene). The sgRNA-coding DNA was then amplified together with the T7 promoter to generate pure templates for *in vitro* transcription using MEGA shortscript Kit (Life Technologies, NY, USA). A Cas9 expression plasmid (Addgene) was linearized with PmeI and used as template for *in vitro* transcription using the T7 Ultra Kit (Life Technologies). Purified *Cas9* mRNA and sgRNAs were mixed and injected into the cytoplasm of fertilized eggs (with clearly evident pronuclei) of C57BL/6 mice in M2 medium (Sigma-Aldrich, MO, USA). Successful knockout was validated by PCR analysis with the following primers: *Chaer* WT-F: 5′-TGAACGCTCTGCAAATCCTA-3′; *Chaer* WT-R: 5′-TAAAGCCAGCAAGAACATAAGG-3′; *Chaer* KO-F: 5′-GGACAGCATCTTCCCTACCACC-3′; *Chaer* KO-R: 5′-CAACCAGTT GGAAGGCCGTAAG-3′. The wild-type allele yielded an amplicon of 155 bp, whereas the mutated allele yielded an amplicon of 317 bp. Out of 26 injected embryos, nine pups were generated and the mutated allele was detected in six. One mouse was selected to mate with the wild-type C57BL/6 strain to obtain F1-generation mice. Heterozygous F1 offspring were interbred to establish the *Chaer*$^{-/-}$ strain.

Transaortic constriction surgery and pressure–volume loop analysis. Transaortic constriction (TAC) surgery was performed as described[22]. Wild-type and *Chaer*-KO male mice at 2 months of age were randomly separated into sham and TAC groups; group information was double blinded between the investigator who performed the surgery and the data analyzer. The mouse was fixed in a supine position with the neck slightly extended. A 20-G catheter was inserted through the larynx into the trachea with care taken not to puncture the trachea or other structures in the pharyngeal region (endotracheal incubation). Ventilation was performed with a tidal volume of 200 μL, respiratory rate of 120/min, 95% oxygen. Body temperature was maintained as close as possible to 37.0 °C throughout the experiment using a self-regulating heating pad. After disinfection with 2% iodine, the chest cavity was opened by an incision of the left second intercostal space. The aortic arch was dissected from the surrounding tissue. The pericardial sac was opened while a 6-0 suture was passed underneath the transverse aorta and ligated over a 27-G needle, which was removed later to provide a lumen. The chest cavity, muscle and skin were closed layer by layer. Sham-operated mice underwent similar surgical procedures, including isolation of the aorta and looping of the aorta, but without tying of the suture. Mice were observed until recovery in a 37.0 °C heated cage.

For the invasive hemodynamic analysis, mice were anesthetized by treatment with 1.5–2% isoflurane, and then a 1.4-FrenchMillar catheter-tip micromanometer catheter (SPR-839; Millar Instruments, Houston, Texas) was inserted through the right carotid artery into the left ventricle of the mice. After stabilization for 15 min, heart rate, pressure and volume signals were recorded continuously with an Aria pressure–volume conductance system coupled to a Powerlab/4SP A/D converter and subsequently were stored and displayed on a computer.

Echocardiography. Transthoracic ultrasonography was performed with a Vevo 2100 system (Fujifilm VisualSonics, Ontario, Canada). Echocardiography was performed before and 4 d after TAC surgery. The inhalational flow of isoflurane was adjusted to anaesthetize the mice while maintaining their heart rate at 450–550 beats/min. The peak aortic blood velocity across the aortic constriction was measured in the pulsed-wave color Doppler mode. Left ventricular function was assessed by M-mode scanning of the left ventricular chamber, standardized by two-dimensional, short-axis views of the left ventricle at the mid papillary muscle level. Left ventricular chamber size and wall thickness were measured for at least three beats from each projection and averaged. Left ventricular internal dimensions at diastole and systole (LVID;d and LVID;s, respectively) were measured.

***In vivo* Chaer silencing.** For *in vivo* gene knockdown, chemically modified siChaer (5′-CCGGACUUGAAUAGUAUAU-3′) and siNeg (CMSINC-30) were designed and synthesized by Bioland Scientific (CA, USA) and delivered into the heart using nanoparticle transfection reagent (Altogen Biosystems, NV, USA) by two injections through the femoral vein each day before (protocol 1) or after (protocol 2) TAC surgery, following the manufacturer's instructions[41]. The efficiency of *Chaer* knockdown in the heart was evaluated by real-time RT–PCR.

Northern blot analysis. Northern blot was performed with the DIG Northern Starter Kit (12039672910, Roche). Briefly, total RNA was extracted from tissues using TRIzol reagents. RNA was quantified by spectrophotometry (NanoDrop 2000 spectrophotometer, Thermo Fisher Scientific, MA, USA) and 1 μg RNA was combined with 4 μl formaldehyde, 10 μl deionized formamide and 2 μl

doi:10.1038/nm.4179

10× MOPS buffer (0.4 M 3 (*N*-morpholino) propanesulphonic acid, 0.1 M sodium acetate, 0.01 M EDTA, pH 7.0) in a total volume of 20 µl. Mouse, rat and normal human heart samples were heated at 85 °C for 10 min, cooled on ice and added to 2 µl 10× RNA loading buffer (50% glycerol, 0.01 M EDTA, pH 8.0, 0.25% (wt/vol) bromophenol blue, 0.25% (wt/vol) xylene cyanol FF), and then the mixture was loaded on a 1.5% agarose, 2.2 M formaldehyde gel. Samples were run at 80 V for 4 h in 1× MOPS buffer. After transfer to a positively charged nylon membrane (Biodyne B Nylon Membrane, Thermo Fisher Scientific, MA, USA) and UV cross-linking, 150 ng of a digoxigenin (DIG)-labeled probe complementary to the target gene was hybridized to the membrane at 68 °C. Probes were synthesized and quantified using a DIG Northern starter kit (12039672910, Roche) as directed by the manufacturer. Washes and detection were carried out as described by the manufacturer, using the reagents supplied in the DIG Northern starter kit. Blots were visualized using Bio-Rad ChemiDoc XRS+ (Bio-Rad). Primers for probe synthesis targeting *Chaer* RNA are listed below: mouse: Forward primer: GTCCGATGCCAGTTCCAGTT; Reverse primer: TAATACGACTCACTATAGGGGCTCCCCTCAGAGTAAAGAG; rat: Forward primer: GGTGAAAGCCTGTGTAGT; Reverse primer: TAATACGACTCACTATAGGGGTAGACTGCTTGAGGGAACAG; human: Forward primer:AGTCACTGCTGTGCTCCATGCCA; Reverse primer: TAATACGACTCACTATAGGGTGCCAGCTTGGGAGGCCTGTA.

Fluorescent *in situ* hybridization. The hearts of male C57BL/6 mice were dissected, immersed immediately in fresh 10% neutral-buffered formalin, fixed for 16 h at room temperature, rinsed briefly, dehydrated and embedded in paraffin. Hearts were cut into transverse sections with a thickness of 6 µm. The TYPE-1 ViewRNA probe against *Chaer* lncRNA (VB1-19372) was designed by Affymetrix and was detected by ViewRNA ISH Tissue Assay Kit (Affymetrix, QVT0012) according to the manufacturer's instructions. Briefly, tissue sections were deparaffinized and then heated in 90–95 °C pretreatment solution for 10 min, followed by protease incubation at 40 °C for 35 min. The TYPE-1 ViewRNA probe against *Chaer* lncRNA was hybridized at 40 °C for 2–4 h. After the preamplifier hybridization, amplifier hybridization and AP-conjugated anti-TYPE-1 ViewRNA probe hybridization steps, probes were visualized by Fast-Red substrate at 40 °C for 40 min. Immunofluorescence assays were performed subsequently to detect cardiac myocytes, endothelial cells and fibroblasts, using antibodies against troponin T type 2 (Tnnt2; Bioworld Technology, BS6013, 1:100), isolectin b4 (ib4; Enzo Life Sciences, ALX-650-001B-MC05, 1:100) and type I collagen (MD Biosciences, 203002, 1:200), respectively. Images were taken with an Olympus FluoView FV1000 confocal laser-scanning microscope.

***In vitro* translation assay.** To validate that *Chaer* is indeed a noncoding RNA, we developed an immunoblotting-based method by combining *in vitro* translation with puromycin incorporation. Briefly, mouse *Chaer* and *Hotair* were cloned into the pCFE1-T7 plasmid (Addgene) and subjected to *in vitro* translation using a human HeLa cell lysate system (1-Step Human High-Yield Mini IVT Kit, Thermo Fisher Scientific). The reaction was carried out following the manufacturer's instructions in the presence of puromycin (Thermo Fisher Scientific, 1 µM), which will be incorporated into any actively translated peptide and facilitates sensitive detection by immunoblotting using anti-puromycin antibody (Sigma-Aldrich, MO, USA; MABE343, 1:1,000). pCFE1-T7-GFP (Addgene) was used as a positive control for translation.

Real-time RT–PCR analysis. Total RNA was extracted from heart tissue or cells using the TRIzol reagent (Life Technologies, NY, USA). 1 µg RNA was reverse-transcribed into first-strand cDNA using the Superscript III first-strand synthesis kit (Life Technologies, NY, USA) with random primers. Real-time PCR was performed using the CFX96 Real-Time PCR Detection System (Bio-Rad, CA, USA) using the iQ SYBR Green Supermix (Bio-Rad). Values were normalized to *Gapdh* to calculate relative expression levels. For fractionation, mouse heart was homogenized in Fraction buffer A containing 10 mM Tris-HCl (pH 7.5), 250 mM sucrose, 0.5 mM EDTA and 0.5 mM EGTA. Cell debris was cleared by centrifugation at 200*g* at 4 °C for 3 min. Nuclei were pelleted at 2,000*g* at 4 °C for 5 min. RNA from the nuclear and cytosolic fractions were extracted with TRIzol and TRIzol LS reagents (Life Technologies, NY, USA) respectively, and subjected to reverse-transcription followed by real-time PCR analysis, as described above. Data are shown as a percentage of the sum between the value in the nuclei and the value in the cytoplasm, and RNA levels were compared to the levels of the nuclear marker *U6* and the cytosolic markers *Rn18S* and *Actb.* All primers are listed in **Supplementary Table 5**.

RNA deep-sequencing and transcriptome analysis. RNA deep-sequencing was performed as described previously[22]. Total RNA was extracted from NRVMs, with or without PE treatment, and with siNeg or siChaer transfection using TRIzol reagents, and it was then reverse-transcribed using the TruSeq RNA Library Prep Kit (Illumina, CA, USA). The libraries were subjected to quality validation using the Agilent Bioanalyzer 2100, and then paired-end sequenced using HiSeq 2500 (Illumina). The resulting reads were mapped to the rn5 database using TopHat2 (ref. 61) and visualized on the UCSC browser (http://genome.ucsc.edu). Gene Ontology (GO) analysis was performed with DAVID Bioinformatics Resources 6.7. Genes with an expression change >1.5-fold were clustered and shown in a heat map (log_2 scale) using NetWalker[62].

Immunoblotting analysis. Immunoblotting analysis was performed as previously described[63]. Cells were washed twice with ice-cold PBS and harvested in protein lysis buffer (50 mM HEPES (pH 7.4), 150 mM NaCl, 1% Triton X-100, 1 mM EDTA, 1 mM EGTA, 1 mM glycerophosphate, 2.5 mM sodium pyrophosphate, 1 mM Na_3VO_4, 20 mM NaF, 1 mM phenylmethylsulfonyl fluoride, 1 mM DTT and 1× complete protease inhibitor tablet (Roche)). Total cell lysates were separated on 4–12% Bis-Tris gels (Life Technologies) and transferred onto PVDF membranes (Merck Millipore). The membranes were probed with antibodies to H3, H3K4me2, H3K9me2, H3K27me2 (#9847 from Cell Signaling Technologies for above antibodies; 1:1,000), H3K27me3 (Cell Signaling Technologies; #9733, 1:1,000), SUZ12 (Cell Signaling Technologies; #3737, 1:1,000), EZH2 (Cell Signaling Technologies; #5246, 1:1,000), RpAb46/48 (Santa Cruz Biotechnology; #33170, 1:1,000), EED (Santa Cruz Biotechnology; #28701, 1:1,000), p-S6K (Thr389, Cell Signaling Technologies; #9234, 1:1,000) and S6K (Cell Signaling Technologies, MA, USA; #9202, 1:1,000). Protein signals were detected using horseradish peroxidase (HRP)-conjugated secondary antibodies and enhanced chemiluminescence (ECL) western blotting detection regents (Thermo Fisher Scientific, MA, USA).

PRC2 histone methyltransferase activity assay. To test the effect of *Chaer* on PRC2 activity, we performed the histone methyltranferase activity assay as previously described[64]. Reactions were carried out in a volume of 50 µL and contained 2 pmol nucleosomes (New England BioLabs, MA, USA), 2 pmol PRC2 complex (Active Motif, CA, USA), 10 mM HEPES (pH 7.9), 0.25 mM EDTA, 200 mM NaCl, 10% glycerol, 2 mM dithiothreitol, 2.5 mM $MgCl_2$ and 0.8 µM *S*-adenosyl-methionine (New England BioLabs, MA, USA), with or without 10 nM *Chaer* RNA or 200 nM EZH2 inhibitor GSK126 (Merck Millipore, Darmstadt, Germany). Reactions were incubated for 2 h at 30 °C, and the reaction products were resolved by SDS–PAGE followed by immunoblotting using anti-H3K27me3 antibody (Cell Signaling Technologies, MA, USA; #9756, 1:1,000).

RNA immunoprecipitation. RNA–protein interactions were validated using RNA immunoprecipitation (RIP), essentially as described[65]. Mouse hearts or cells were homogenized in adequate volumes of polysome lysis buffer (10 mM HEPES-KOH (pH 7.0), 100 mM KCl, 5 mM $MgCl_2$, 25 mM EDTA, 0.5% IGEPAL, 2 mM dithiothreitol (DTT), 0.2 mg/mL Heparin, 50 U/mL RNase OUT (Life Technologies, NY, USA), 50 U/mL Superase IN (Ambion) and 1× complete protease inhibitor tablet (Roche)). The suspension was centrifuged at 14,000*g* at 4 °C for 10 min to remove debris. Lysates containing 1 mg protein were incubated with 500 ng normal IgG (Cell Signaling Technologies, MA, USA; #2729, 1:200), anti-SUZ12 (Cell Signaling Technologies, MA, USA; #3737, 1:200), anti-EZH2 (Cell Signaling Technologies, MA, USA; #5246, 1:200), anti-WDR5 (Abcam, Cambridge, UK; #56919, 1:200), or anti-LSD1 (Cell Signaling Technologies, MA, USA; #2139, 1:200) at 4 °C overnight on an inverse rotator. Protein A–sepharose beads (Life Technologies, 50 µL per tube) were first blocked in NT2 buffer (50 mM Tris-HCl (pH 7.5), 150 mM NaCl, 1 mM $MgCl_2$ and 0.05% IGEPAL) supplemented with 5% BSA, 0.02% sodium azide and 0.02 mg/mL heparin at 4 °C for 1 h, and then added into the lysates followed by a 3-h incubation at 4 °C on an inverse rotator. The beads were subsequently washed five times in NT2 buffer. RNAs were released by incubating in proteinase K buffer (50 mM Tris (pH 8.0),

100 mM NaCl, 10 mM EDTA, 1% SDS and 1 U/mL proteinase K) for 30 min at 65 °C, and pelleting by adding an equal volume of isopropanol and centrifuging at 12,000*g* at 4 °C for 10 min. After washing once with 75% ethanol, RNAs were reverse-transcribed into first-strand cDNA and used for real-time RT–PCR analysis to detect the indicated lncRNAs. *Hotair* lncRNA was tested as a positive control for SUZ12 and LSD1 binding, and *Hottip* lncRNA was used as a positive control for WDR5 binding. Data were normalized to IgG control groups.

Tagged-RNA pulldown. To identify the direct binding partners of *Chaer*, we used a tagged-RNA pulldown assay, as previously described[66]. Sense and antisense strands of streptavidin-binding S1m DNA were synthesized by Life Technologies Inc., annealed and cloned into pcDNA5-CMV in front of a cloning site into which was inserted sequences encoding wild-type or truncated versions of *Chaer*; truncations were made at roughly 500-bp intervals from either the 5′ or 3′ end. These constructs, as well as those expressing untagged wild-type *Chaer* and EGFP, were transfected into MEFs for 48 h. Cells were then harvested in SA-RNP lysis buffer (20 mM Tris-HCl (pH 7.5), 150 mM NaCl, 1.5 mM $MgCl_2$, 2 mM DTT, 50 U/mL RNase OUT (Life Technologies, NY, USA), 50 U/mL Superase IN (Ambion) and 1× complete protease inhibitor tablet (Roche)). Streptavidin–sepharose beads were blocked with 500 ng/μL yeast tRNA and 1 mg/mL BSA in SA-RNP lysis buffer before being added into cell lysates and being incubated at 37 °C for 2 h on a rotator. The beads were then pelleted and washed five times with SA-RNP washing buffer (20 mM Tris-HCl (pH 7.5), 300 mM NaCl, 5 mM $MgCl_2$, 2 mM DTT, 50 U/mL RNase OUT (Life Technologies, NY, USA), 50 U/mL Superase IN (Ambion) and 1× complete protease inhibitor tablet (Roche)). After the last wash, RNA-bound proteins were eluted by addition of 5% RNase A (New England BioLabs, MA, USA) in low-salt buffer (20 mM Tris-HCl (pH 7.5), 30 mM NaCl, 5 mM $MgCl_2$, 2 mM DTT and 1× complete protease inhibitor tablet (Roche)) for 30 min at 4 °C. The eluted proteins were then boiled in 4× LDS sample buffer (Life Technologies) and used for immunoblot analysis.

RNA electrophoretic mobility shift assay (EMSA). RNA electrophoretic mobility shift assay (EMSA) assay was performed essentially as described[30]. RNA probes were synthesized from linearized pBluescript-Chaer-66-mer and pBluescript-Hotair-89-mer using RiboMAX Large-Scale RNA Production Systems (Promega, WI, USA), and labeled with biotin using the RNA 3′ End Biotinylation Kit (Thermo Fisher Scientific) following the manufacturer's instructions. Recombinant EZH2 was expressed from linearized pT7CFE1-Ezh2 (Addgene) in a coupled transcription and translation system (1-Step Human *In vitro* Protein Expression Kits, Thermo Fisher Scientific) following the manufacturer's instructions. RNA EMSA was performed by using the LightShift Chemiluminescent RNA EMSA Kit (Thermo Fisher Scientific). For each reaction, 10 pmol of labeled probe was incubated with 1 μL out of 20 μL *in vitro*–translated EZH2 in the presence of tRNA (1 mg/mL) at room temperature for 30 min. Unlabeled probes at indicated concentrations were used for competition experiments. The reactions were then loaded onto a 1% 0.5× TBE–agarose gel and transferred to a positively charged nylon membrane (Roche). The membrane was then cross-linked by exposure to UV, incubated with HRP-conjugated streptavidin and visualized with ECL reagents. The dissociation constant (K_d) was calculated as the concentration of unlabeled probe when half of the labeled probe was dissociated from the complex with EZH2.

Chromatin immunoprecipitation (ChIP)-PCR assay. Chromatin immunoprecipitation (ChIP) assay was performed to evaluate PRC2 targeting and H3K27me3 levels at specific promoters as described[67,68]. Briefly, minced hearts or NRVMs were fixed with 1% formaldehyde for 10 min at room temperature and then quenched by addition of 125 mM glycine. The samples were homogenized in lysis buffer (containing 20 mM Tris-HCl (pH 8.0), 150 mM NaCl, 2 mM EDTA, 1% Triton X-100, 0.1% SDS and 1× complete protease inhibitor tablet) and sonicated to generate chromatin samples with average fragment sizes of 200–1,000 bp. After preclearing with Protein A–sepharose beads, samples were incubated with anti-H3K27me3 antibody (Cell Signaling Technologies, MA, USA), anti-EZH2 (Cell Signaling Technologies (#5246) for ChIP in mouse hearts; Santa Cruz Biotechnology (#292275) for ChIP in NRVMs) or normal control IgG at 4 °C overnight on an inverse rotator. Antibody–chromatin complexes were then pelleted with Protein A–sepharose beads that had been blocked with BSA and salmon sperm DNA. After standard washes, the immunoprecipitated DNA was eluted and purified with PCR purification kit (Qiagen). RT–PCR was then performed using primers targeting the promoter regions of hypertrophy-related genes, as listed in **Supplementary Table 5**.

Histology, trichrome staining and PicroSirius Red staining. Histology (H&E) and trichrome (Masson's) staining were performed as previously described[69,70]. Mouse hearts from the sham, TAC–siNeg or TAC–siChaer groups were perfused and fixed with 10% formalin before embedding in paraffin. Embedded hearts were sectioned into 5-μm-thick slices as cross-sections at the midpoint of the ventricle. To evaluate the effect of *Chaer* on fibrosis after TAC surgery, collagen was stained with PicroSirius Red (PSR) following the manufacturer's instructions (Abcam, Cambridge, UK)[71]. Sections were imaged with a SPOT digital camera system (Diagnostic Instruments, Sterling Heights, MI, USA), and fibrosis area was measured with a quantitative digital image analysis system (Image-Pro Plus 6.0). Cross-section cell size was measured from at least four hearts from each group with about 20 cells analyzed per section.

***In silico* prediction for RNA structure and protein–RNA interaction.** For translational-propensity analysis of an RNA sequence, the predicted peptides over 30 amino acids in all three potential reading frames were searched using PFAM 27.0 (ref. 33). RNA secondary structure was predicted by RNAfold WebServer (http://rna.tbi.univie.ac.at/cgi-bin/RNAfold.cgi) based on minimum free energy (MFE) and partition function. The binding propensity between EZH2 and RNA fragments was predicted using catRAPID (http://s.tartaglialab.com/page/catrapid_group). Gene ontology (GO) analysis was performed using David Bioinformatics Resources 6.7 (https://david.ncifcrf.gov/).

Statistical analysis. Comparisons in multiple groups were analyzed with one-way ANOVA, followed by Student's *t*-test to calculate the *P* value between two groups. The sample size was determined by holding the probability of a type I error at $\alpha = 0.05$. Correlation analysis was done by Pearson's *r* test. Data are presented as mean ± s.e.m. or s.d. for triplicates.

55. National Research Council. *Guide for the Care and Use of Laboratory Animals* 8th edn. (The National Academies Press, 2011).
56. MacLellan, W.R., Xiao, G., Abdellatif, M. & Schneider, M.D. A novel Rb- and p300-binding protein inhibits transactivation by MyoD. *Mol. Cell. Biol.* **20**, 8903–8915 (2000).
57. van Laake, L.W. *et al.* Reporter-based isolation of induced pluripotent stem cell– and embryonic stem cell–derived cardiac progenitors reveals limited gene expression variance. *Circ. Res.* **107**, 340–347 (2010).
58. Ubil, E. *et al.* Mesenchymal–endothelial transition contributes to cardiac neovascularization. *Nature* **514**, 585–590 (2014).
59. Zhou, Y.Y. *et al.* Culture and adenoviral infection of adult mouse cardiac myocytes: methods for cellular genetic physiology. *Am. J. Physiol. Heart Circ. Physiol.* **279**, H429–H436 (2000).
60. Wang, H. *et al.* One-step generation of mice carrying mutations in multiple genes by CRISPR–Cas-mediated genome engineering. *Cell* **153**, 910–918 (2013).
61. Langmead, B. & Salzberg, S.L. Fast gapped-read alignment with Bowtie 2. *Nat. Methods* **9**, 357–359 (2012).
62. Komurov, K., Dursun, S., Erdin, S. & Ram, P.T. NetWalker: a contextual network analysis tool for functional genomics. *BMC Genomics* **13**, 282 (2012).
63. Lu, G. *et al.* Protein phosphatase 2Cm is a critical regulator of branched-chain amino acid catabolism in mice and cultured cells. *J. Clin. Invest.* **119**, 1678–1687 (2009).
64. Nekrasov, M., Wild, B. & Müller, J. Nucleosome-binding and histone methyltransferase activity of *Drosophila* PRC2. *EMBO Rep.* **6**, 348–353 (2005).
65. Baroni, T.E., Chittur, S.V., George, A.D. & Tenenbaum, S.A. Advances in RIP-chip analysis: RNA-binding protein immunoprecipitation–microarray profiling. *Methods Mol. Biol.* **419**, 93–108 (2008).
66. Leppek, K. & Stoecklin, G. An optimized streptavidin-binding RNA aptamer for purification of ribonucleoprotein complexes identifies novel ARE-binding proteins. *Nucleic Acids Res.* **42**, e13 (2014).
67. Sdek, P. *et al.* Rb and p130 control cell cycle gene silencing to maintain the postmitotic phenotype in cardiac myocytes. *J. Cell Biol.* **194**, 407–423 (2011).
68. Young, M.D. *et al.* ChIP-seq analysis reveals distinct H3K27me3 profiles that correlate with transcriptional activity. *Nucleic Acids Res.* **39**, 7415–7427 (2011).
69. Streicher, J.M., Kamei, K., Ishikawa, T.O., Herschman, H. & Wang, Y. Compensatory hypertrophy induced by ventricular-cardiomyocyte-specific COX-2 expression in mice. *J. Mol. Cell. Cardiol.* **49**, 88–94 (2010).
70. Mitchell-Jordan, S.A. *et al.* Loss of Bmx nonreceptor tyrosine kinase prevents pressure-overload-induced cardiac hypertrophy. *Circ. Res.* **103**, 1359–1362 (2008).
71. Jiang, D.S. *et al.* Interferon regulatory factor 7 functions as a novel negative regulator of pathological cardiac hypertrophy. *Hypertension* **63**, 713–722 (2014).

doi:10.1038/nm.4179